

DOI: 10.1002/adem.201000106

# Spark Plasma Sintering, Microstructures, and Mechanical Properties of Macroporous Titanium Foams\*\*

By Faming Zhang\*, Eileen Otterstein and Eberhard Burkel

*Macroporous pure titanium (Ti) foams with porosity of 30–70% and pore size of 125–800  $\mu\text{m}$  were fabricated by using spark plasma sintering (SPS) and NaCl dissolution methods. A mixture of Ti and sodium chloride (NaCl) powders were spark plasma sintered in a temperature range from 550 to 800 °C and the NaCl phase was then dissolved in water. High purity Ti foams were obtained at the SPS temperature of 700 °C for holding time of 8 min under pressure of 50 MPa. The resulting Ti foams consist of pure  $\alpha$ -Ti phase with interconnected macropores in square cross sections. The plateau stress and Young's modulus agree with the Gibson–Ashby models, and coarsely follow of linear decline with the increase of the pore sizes, and exponential decay with the increase of the porosity. The macroporous Ti foams with plateau stress 27.2–94.2 MPa and Young's modulus 6.2–36.1 GPa may have a potential to be used as bone implants.*

Porous materials with interconnected porosity have widespread applications in many fields of engineering.<sup>[1]</sup> Bulk porous metallic materials (honeycomb, foam, and hollow spheres) are known for their interesting combinations of the advantages of a metal (strong, hard, tough, electrically, and thermally conductive, etc.) with the functional properties of porous structures (lightweight with adjustable properties by selecting the density).<sup>[2]</sup> Because of this, porous metals are interesting for a number of engineering applications such as structural panels, energy absorption devices, acoustic damping panels, compact heat exchangers, and biomedical implants etc.<sup>[3]</sup> Porous titanium (Ti) and its alloy were widely used in the biomedical field due to their outstanding mechanical properties, low density, chemical resistance, and biocompatibility. As a kind of long-term load-bearing implant, the porous structures of Ti and its alloy could lead to a reliable anchoring of host tissue into the porous structure, and allow mechanical interlocking between bone and implant.<sup>[4]</sup> The ingrowths of bone into the porous structure could ensure a good transfer of mechanical forces. Therefore, a

porous structure is preferable for the Ti and its alloys using as bone scaffolds.

However, porous Ti and its alloys are difficult to be produced from the liquid state, due to the high melting point, the high reactivity at high temperature above 1000 °C and the contamination susceptibility. Thus, fabrication processes for porous Ti has to date focused on the powder metallurgy (PM) route and avoided the liquid route.<sup>[5]</sup> Many techniques have been applied to produce porous Ti and its alloy implants in recent years.<sup>[6–10]</sup> Nevertheless, there are still problems to be solved in the field of porous Ti for biomedical applications<sup>[11]</sup>: the difficulty to create controlled porosity and pore sizes, the insufficient knowledge of porous structure–property relationships, the requirements of new sintering techniques with rapid energy transfer, and less energy consumption and so on.

Spark plasma sintering (SPS) as one of the field assisted sintering techniques, is a relative new sintering technique for PM and ceramics. SPS is a high efficient and energy saving powder consolidation and sintering technology capable of processing conductive and non-conductive materials.<sup>[12]</sup> However, most of SPS researches were performed on dense materials; fewer studies were on porous materials.<sup>[13]</sup> The SPS studies on porous Ti alloys were mainly using low temperature and low pressure to decrease the relative density of samples.<sup>[14–19]</sup> The samples exhibited pore sizes of some tens of micrometers and a porosity in the range of 20–45%. As bone foams, high porosity (>50%) and macropore size (>200  $\mu\text{m}$ ) are essential requirements for the bone growth and the osteoconduction.<sup>[20,21]</sup> Macroporous nanostructured tricalcium phosphate scaffolds have been successfully

[\*] Dr. F. Zhang, E. Otterstein, Prof. Dr. E. Burkel  
Institute of Physics, University of Rostock, August Bebel Str. 55,  
D-18055 Rostock, Germany  
E-mail: faming.zhang@uni-rostock.de

[\*\*] This research was supported by the DFG-Deutschen Forschungsgemeinschaft (German Research Foundation) with grant no. GRK1505/1 (Welisa). The authors acknowledge the FCT systeme GmbH for the support in SPS experiments, and Prof. R. Balder in the Department of orthopedic of University Rostock for his support in mechanical testing.

prepared by using SPS with a special die design.<sup>[21]</sup> Nevertheless, macroporous Ti foams by SPS were scarcely reported.

The spacer method was developed to fabricate porous metals and ceramics since 1960s. The method can control the pore characteristics by adjusting of the mixing ratio and the particle size of spacer.<sup>[22]</sup> The sodium chloride (NaCl) has been used as spacer material for aluminum<sup>[23]</sup> and Ti alloys<sup>[24,25]</sup> due to its relative high melting point (801 °C), its low cost, and the easy dissolution in water, the less corrosive attack of metals and the low toxicity. The combination of the SPS technique with the NaCl dissolution were tried in aluminum metals at SPS temperature of 570 °C,<sup>[26,27]</sup> and the processed porous aluminum demonstrated high sound absorption property.<sup>[28]</sup> In fact, Ti has a much higher melting point (1660.0 °C) than aluminum (660.3 °C). Therefore, it is a great challenge to fabricate Ti foams by using the SPS and NaCl dissolution methods.

The objective of this study is to develop macroporous Ti foams with controlled architectures using the SPS in combination with the NaCl dissolution methods. The major parameters involved in the preparation process were studied. The microstructures of the prepared foams were analyzed by using 3D X-ray microcomputed tomography (micro-CT) and scanning electron microscopy (SEM) techniques. The relationship between the mechanical properties and the porous architectures were analyzed and discussed.

### Experimental

#### Raw materials

The precursor Ti powders were prepared by hydride-dehydride method with 99.5% purities in 325 meshes (Alfa Aesar, Germany). The space holder material consisted NaCl crystalline powders with 99.0% purity (Alfa Aesar) sieved in the range of 100–1000 μm.

#### Pore forming method

The Ti powders and NaCl powders were homogeneously mixed in different weight ratios in a blender with paraffin wax as a binder. The mixtures were loaded into graphite die with graphite paper between the punches and die to sinter disc-shaped pellets (20 mm diameter, thickness 6–7 mm). The SPS experiments were performed using a Model HPD-25/1 FCT SPS system (FCT systeme GmbH, Rauenstein, Germany) at temperatures of 550–800 °C lasting for various time. During the experiments, the temperature is measured by a central pyrometer with a focus point at the bottom of the central borehole of the graphite set-up, 2.88 mm from the bottom of the upper punch and 5.125 mm from the center of a 4.25 mm thick sample inside the die<sup>[29]</sup>. The temperature of the die is measured by a second two-color pyrometer, focused on the outer die wall surface at the same height as the center of the compact. The applied direct current for SPS was about 1000–2000 A (voltage < 5 V) with a pulse duration of 12 ms and an interval of 2 ms. The SPS experiments were conducted in vacuum (<6 Pa) under an uniaxial pressure of 30–50 MPa. The

heating rate was maintained at 100 °C min<sup>-1</sup>. The SPSed samples were then suspended in circulating hot water (80 °C) to dissolve the NaCl space holder for 12 h. The leached Ti forms were cleaned in an ultrasonic water bath for 15 min, rinsed with ethanol and furnace dried at 120 °C for 10 h.

#### Microstructures analysis

X-ray diffraction (XRD, Bruker D8, Germany) was used to characterize the phase composition of the powders and sintered foams with Cu K $\alpha$  radiation (0.154178 nm). The pore structure of the Ti foam was examined by using X-ray micro-CT (GE, USA). The specimens were mounted on a rotary stage and scanned in their entirety, being rotated by 360° in 1400 equiangular steps (4 pics per 1°). The detector size is 2284 pixel in *x* and *y* and 2304 pixel in *z* direction. The voxel size of the images is 10.2 μm in all three axes. The macroporous structures and the microstructures of the obtained Ti foams were analyzed by using a SEM (Zeiss Supra 25, Germany) equipped with EDX. The contents of oxygen and carbon in the Ti foams were evaluated by inert gas fusion techniques using a LECO TCH-600 analyzer.

#### Properties measurements

The porosities and densities of the sintered porous Ti samples were determined by the Archimedes principal method, i.e. the porosity was calculated from the dry weight of the specimen in ambient air, the wet weight of the specimen in ambient air after boiling water impregnation, and the wet weight of the specimen under water after boiling water impregnation. The mechanical behavior of the porous Ti foams was investigated by uniaxial compression experiments at room temperature. The plateau stress measurements were carried out on a universal testing machine Zwick Roell Z050, equipped with a 50 kN load cell at 0.5 mm min<sup>-1</sup>. The strain was measured with a strain gauge. The Young's modulus was calculated by dividing the plateau stress by the plateau strain.

### Results and Discussions

#### Pore Forming Process

Figure 1 shows the SEM micrographs of the starting Ti and NaCl powders. The Ti powders have irregular morphologies and size distribution of 10–30 μm (Fig. 1a). These NaCl powders have cuboid shapes with round angles and size distribution of 150–300 μm, which is according to the sieved size of 100–50 mesh [Fig. 1(b)].

Figure 2 shows the schematic illustration of the pore forming process by using the SPS and NaCl dissolution methods. The Ti and NaCl powders were sieved to the required particle size, firstly [Fig. 2(a)]. Then, the Ti and NaCl powders with different weight ratios were mixed thoroughly [Fig. 2(b)]. Additionally, the Ti/NaCl mixtures were subjected to SPS at various parameters [Fig. 2(c)]. The spark plasma sintered samples were suspended in circulating hot water (80 °C) for as long as 12 h [Fig. 2(d)].

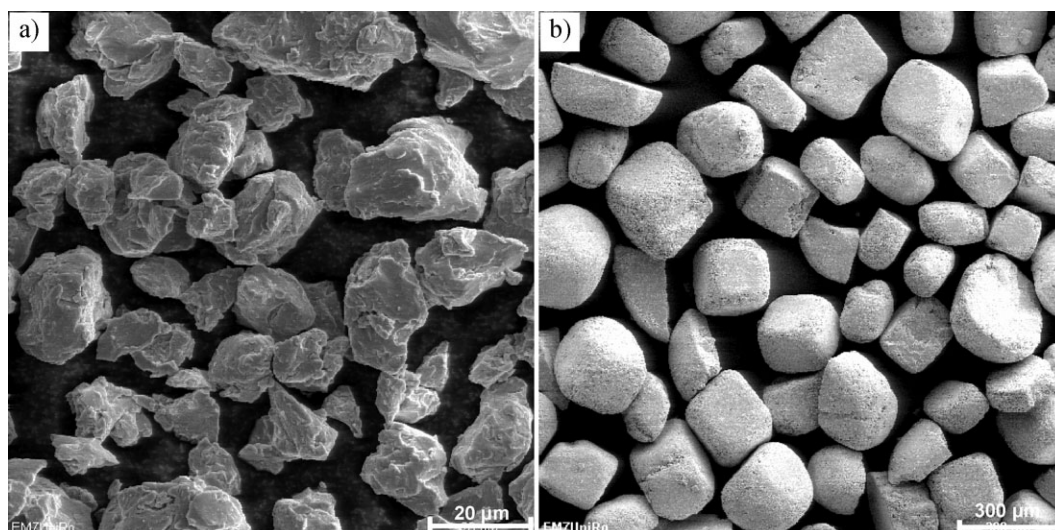


Fig. 1. SEM micrographs of the starting Ti (a) and NaCl (b) powders.

After cleaning and drying, the porous Ti foams were obtained finally [Fig. 2(e)].

The influence of the weight ratio and particle size of NaCl on the porosity and pore size of Ti foams with corresponding SPS parameters is shown in Table 1. The pore sizes of the sintered foams were measured from the SEM images. It shows mean pore sizes about 125 μm in the foams with a NaCl spacing material in the range of 88–149 μm, mean pore size about 250 μm with NaCl of 224–297 μm, 400 μm with NaCl of 388–500 μm sizes, 800 μm with NaCl of 784–1000 μm sizes. After porosity characterization by the Archimedes method, it is noticed that more NaCl particles were needed to obtain the same porosity in the large pore sized foams. To achieve a porosity of 55% in the 125 μm foams, the weight ratio of Ti/NaCl is about 1:1.28. However, the weight ratio of Ti/NaCl is about 1:1.75 in the 800 μm foams for the same porosity. It might be due to the decreased specific surface area in the large sized NaCl particles as spacer materials.

The Ti/NaCl mixtures (Ti/NaCl = 1:1.32) were spark plasma sintered at temperatures of 550–800 °C under a pressure of 30–50 MPa. The exact SPS parameters are shown

in Table 1. The SPSed samples at 750 and 800 °C were failed because of the melting of NaCl particulates resulting in an explanation of the mixture and breakage of the graphite die. The parameters were adjusted, and the Ti foams were prepared by the SPS at conditions of 730 °C for 8 min under 30 MPa. However, the XRD result in Figure 3 shows that there are some rutile TiO<sub>2</sub> phases (PDF#21-1276) and few TiCl<sub>2</sub> phase (PDF#10-0315) in the 730 °C sintered foams. The presences of TiO<sub>2</sub> and TiCl<sub>2</sub> are due to the reaction of the Ti with oxygen and dissociated Cl<sup>-</sup> in NaCl. It is likely that the temperature at the necks of the Ti particles exceeds 730 °C due to the high local contact resistance. Hence NaCl is able to melt causing contamination of the sample. High purity Ti foams were prepared at 700 °C for 8 min under 50 MPa. The starting Ti powders are in the α-Ti phase with hexagonal structure. The Ti foams remain in the α-Ti phase structure without any impurities when the SPS process temperatures are below 700 °C. There is usually some temperature difference between the mold surface and the actual temperature in the SPS sample. The temperature measurement design in the FCT SPS system allowed a very accurate temperature control since the temperature difference between the center of the sample and the controlling pyrometer was always below 5 °C.<sup>[30]</sup> The radial temperature gradient in the electrical conductive samples is about 79 °C around.<sup>[29]</sup> The Ti powders are electrical conductive materials. The sintering temperature of 700 °C plus the temperature difference 5 °C and temperature gradient 79 °C was still lower than the melting point of NaCl (801 °C). Thus, high purity Ti foams can be prepared at the SPS temperature of 700 °C.

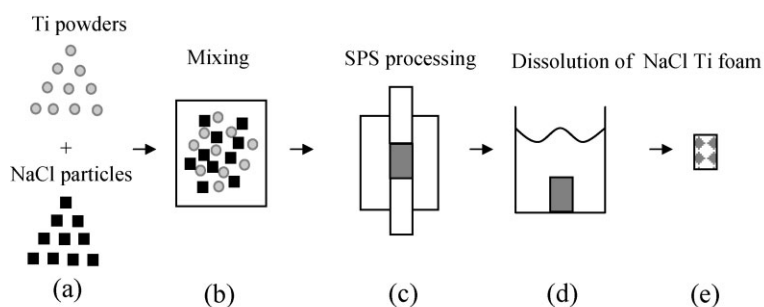


Fig. 2. Schematic illustration of the pore forming process by using the SPS and NaCl dissolution: sieving of the Ti and NaCl powders (a), mixing of the Ti and NaCl powders (b), processing by the SPS (c), dissolution of the NaCl in water (d), obtaining of the Ti foams (e).

### Microstructures

The 3D reconstruction by topographical methods is the most realistic way to get space information

Table 1. The influence of the weight ratio and particle size of NaCl on the porosity and pore size of the Ti foams with corresponding SPS parameters.

Ti powder	NaCl powder	Weight ratio (Ti: NaCl)	Porosity	Pore size	SPS parameters (Temperature, dwell time)
10–30 μm	88–149 μm (170–100 mesh)	1:1.28	~55%	~125 μm	700 °C, 8 min
10–30 μm	149–297 μm (100–50 mesh)	1:0.72	~30%	~250 μm	700 °C, 8 min
		1:0.93	~45%	~250 μm	700 °C, 8 min
		1:1.32	~55%	~250 μm	550 °C, 8 min
					600 °C, 8 min
					650 °C, 8 min
					700 °C, 8 min
					730 °C, 8 min
					750 °C, 5 min
					800 °C, 3 min
		1:1.64	~70%	~250 μm	700 °C, 8 min
10–30 μm	354–500 μm (45–35 mesh)	1:1.46	~55%	~400 μm	700 °C, 8 min
10–30 μm	707–1000 μm (25–18 mesh)	1:1.75	~55%	~800 μm	700 °C, 8 min

about the internal structure of the foams in a non-destructive way. The micro-CT 3D reconstructions of the spark plasma sintered Ti foams with 55% porosity and 250 μm pore size are shown in Figure 4. The 3D cropped isometric view of cross sections in the Ti foam shows the uniform pore distribution and interconnected 3D porous structures with a high porosity [Fig. 4(a)]. The micro-CT 2D top view and side views show that the macropore shapes are in square cross sections, uniform distribution of pore sizes and high interconnectivity [Fig. 4(b–d)]. The 3D surface, cell wall thickness, connectivity were examined by the micro-CT in a non-destructive way. The 3D cropped internal surface exhibits highly porous structures and interconnectivity with pore size of  $243 \pm 50 \mu\text{m}$  and cell wall average thickness  $20.4 \mu\text{m}$ .

The SEM micrographs of the Ti foams with the same porosity of 55% but different pore sizes of 125, 250, 400, and 800 μm is shown Figure 5. All the foams from 125 to 800 μm exhibit highly interconnected porous structures

and uniform pore distribution. It is found that the pores have irregular quadrate cross sections. They are similar to those of the initial NaCl particles of cuboid shapes in Figure 1(b).

Figure 6 shows the SEM micrographs of the porous Ti foams with the same pore size of 250 μm but different porosity of 30, 45, 55 and 70%. The thickness of the pore walls in the 30% porosity foams is about 100 μm, decreasing to 50 μm in 45% porosity foams, and to 20 μm in 55%, finally ending at 10 μm in 70% porosity foams. The interconnectivity was also enhanced with the increase in porosity. The 30 and 45% porosity foams show poor interconnectivity because of the lower porosity [Fig. 6(a and b)]. But the 55 and 70% higher porosity samples showed good interconnectivity [Fig. 6(c and d)]. The macropores are in square cross sections in all the Ti foams with different porosities.

Figure 7 shows the SEM microstructures of the polished cross-section, pore edge, and pore wall of the Ti foams, and EDX analysis on the pore matrix. Few micropores ranged 1–2 μm were detected in the SEM micrograph of the polished cross-section of the Ti foam [Fig. 7(a)]. It is indicated that the Ti foams have been densified after SPS at 700 °C for 8 min under 50 MPa. When polishing porous metals, the pores have to be filled with resin. This prevents release of particles, which cause the rough finish seen in the Figure 7(a). Furthermore it prevents the smaller pores from being filled with debris. The typical pore edge and wall of the Ti foams are shown in Figure 7(b and c). The grain sizes of the Ti foams still range about 10–30 μm without rapid grain growth due to the rapid sintering of SPS. There are some micropores smaller than 10 μm on the pore walls. The micropores could allow body fluid circulation whereas the macropores may provide a scaffold for bone–cell colonization. The surfaces of the pore walls of the macropores of the porous Ti are relatively rough. The EDX analysis shows that the matrix of the pore wall contains only Ti elements

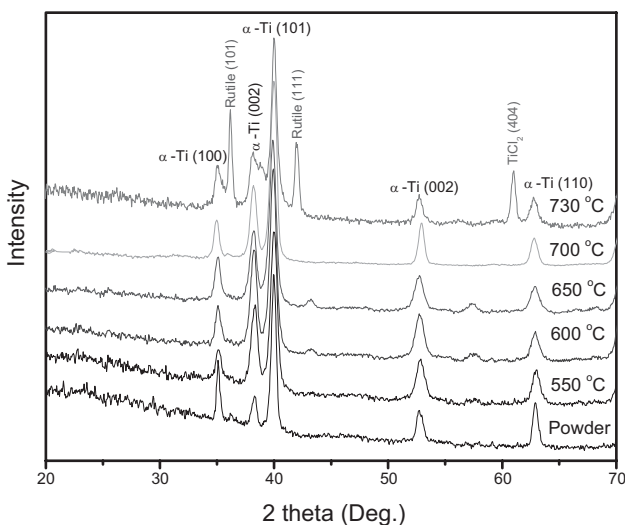


Fig. 3. XRD patterns of the raw Ti powder and Ti foams processed by SPS at 550, 600, 650, 700, and 730 °C.

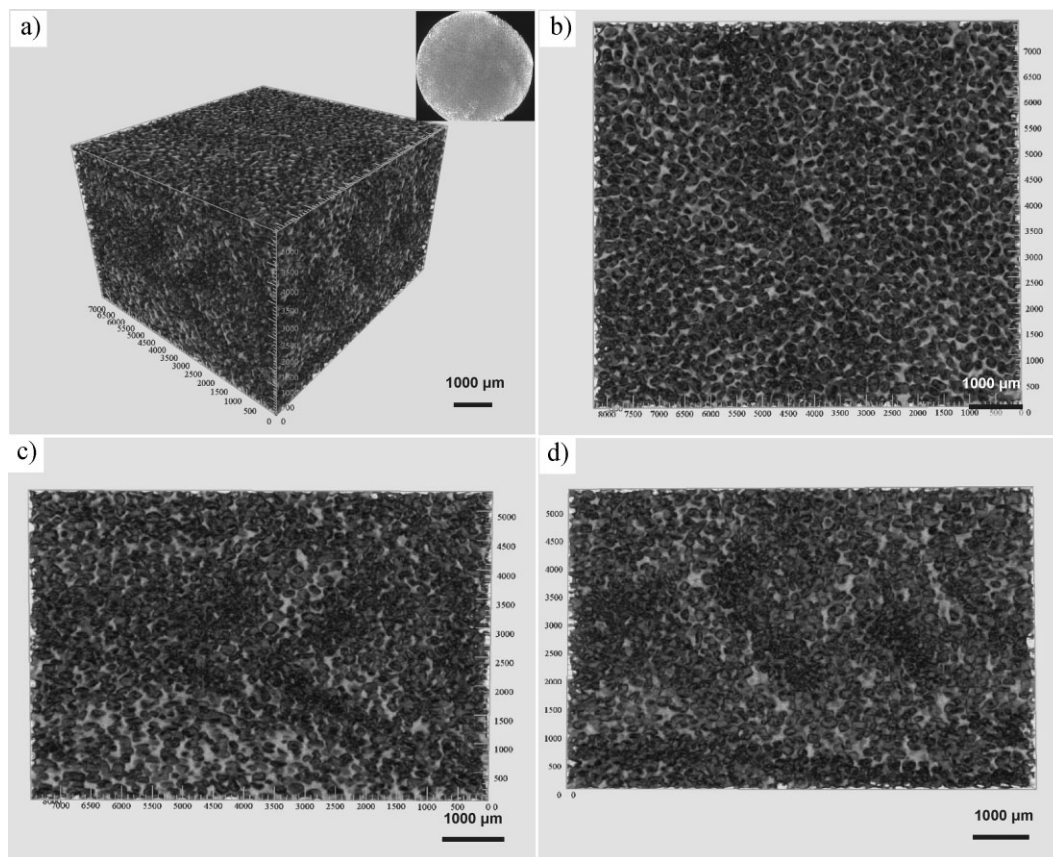


Fig. 4. Micro-CT 3D reconstructions of the Ti foam (250  $\mu\text{m}$  of pore size, 55% of porosity) exhibiting the isometric view of cross sections with a sample navigation (top-right corner) (a), 2D top view (b), left side view (c), and right side view (d).

without O element [Fig. 7(d)]. The chemical analysis by inert gas fusion technique shows that the final C contents in these SPSed Ti foams are  $0.08 \pm 0.02$  wt%, and O contents are  $0.29 \pm 0.04$  wt%. It is between the Grade 2 (C: 0.10 wt%, O: 0.25 wt%) and Grade 3 (C: 0.10 wt%, O: 0.35 wt%) Ti. They are accordingly to the XRD results in Figure 3 that high purity Ti foams were prepared by SPS at 700 °C.

#### Mechanical Properties

Figure 8 shows the effect of pore size and porosity on the plateau stress and Young's modulus of the porous Ti foams. The measured plateau stress and Young's modulus of the Ti foams were compared with the theoretical values that calculated from Gibson–Ashby model. According to the Gibson–Ashby model, the relationship between the relative plateau stress and relative density is given by<sup>[31]</sup>:

$$\frac{\sigma}{\sigma_0} = C \left( \frac{\rho}{\rho_0} \right)^{3/2} \quad (1)$$

where  $\sigma$  is the plateau stress of the foams,  $\sigma_0$  the yield stress of the dense material; C the constant 0.3 from the data of cellular metals and polymers,  $\rho$  is the density of the foams,  $\rho_0$  is the density of the dense material. The density of the pure Ti

is  $4.5 \text{ g cm}^{-3}$  with yield stress of 692 MPa.<sup>[31,32]</sup> The density of the Ti foam with 55% porosity and 250  $\mu\text{m}$  pore size is  $1.69 \text{ g cm}^{-3}$ . Substituting these values in Equation (1), the theoretical value was calculated to be 47.78 MPa, which is comparable to the measured plateau stress  $45.1 \pm 3.0$  MPa. According to the Gibson–Ashby model, the relationship between the relative Young's modulus and relative density is given by<sup>[31]</sup>:

$$\frac{E}{E_0} = A \left( \frac{\rho}{\rho_0} \right)^2 \quad (2)$$

where  $E$  is the Young's modulus of the foams,  $E_0$  the Young's modulus of the dense materials,  $A$  the constant of one including data of metals, rigid polymers, elastomers, and glasses. The Young's modulus of the pure Ti is 105 GPa according to the Equation (2).<sup>[31,32]</sup> The measured Young's modulus of the above Ti foams with 55% porosity is  $13.46 \pm 1.4$  GPa. Substituting the values into Equation (2), it is calculated that the theoretical value is 14.81 GPa which is also comparable to the measured one. All the Ti foams prepared by the SPS were measured and calculated. As seen from the Figure 8, it can be deduced that all the experimental data agrees with the Gibson–Ashby model (1) and (2) in the present study. The relationship between the pore sizes and the mechanical properties of the

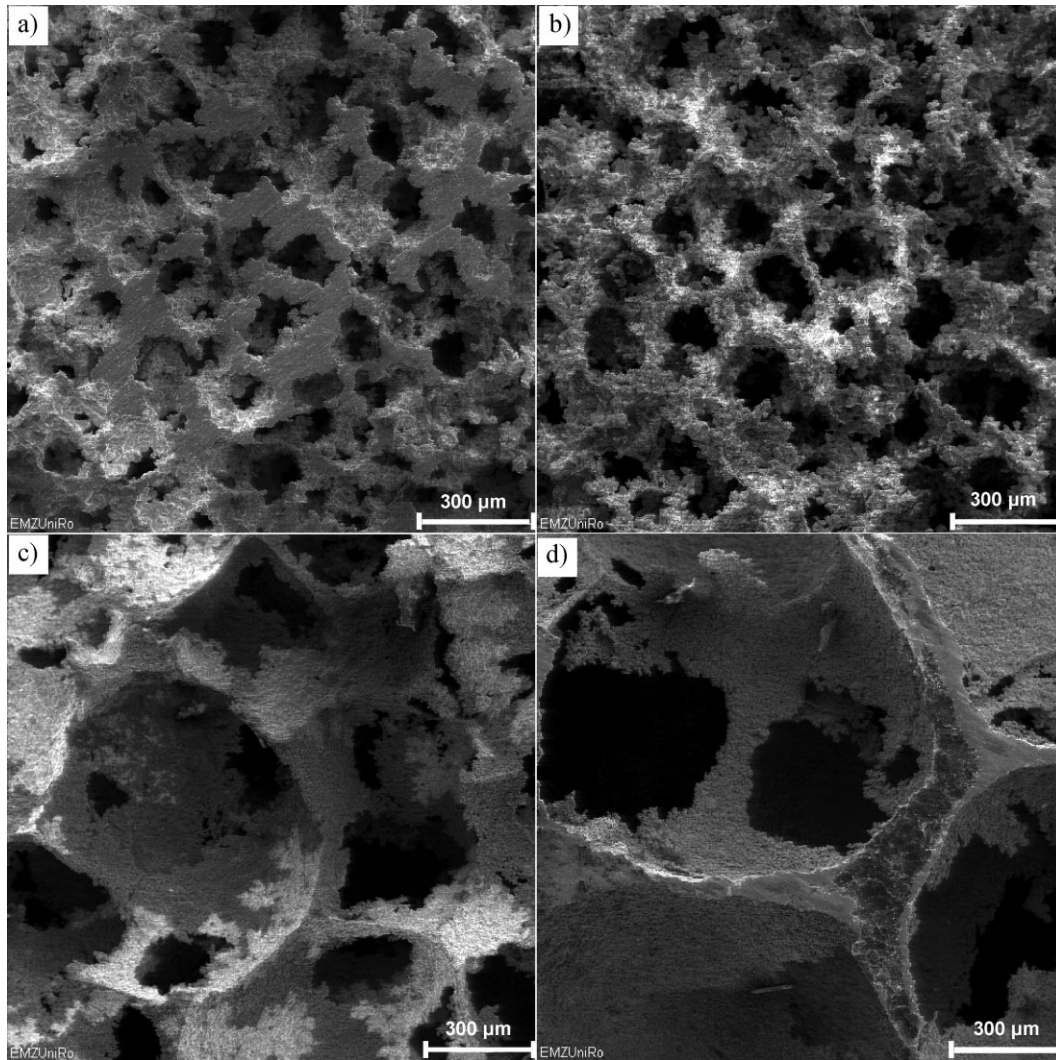


Fig. 5. SEM micrographs of the Ti foam surfaces with the same porosity of 55% but different pore sizes of 125 (a), 250 (b), 400 (c), and 800  $\mu\text{m}$  (d).

Ti foams is shown in Figure 8(a and b). The plateau stress decreased from  $49.7 \pm 3.8$  to  $27.2 \pm 3.0$  MPa with the pore size increase [Fig. 8(a)]. The Young's modulus reduced from  $18.3 \pm 2.0$  to  $8.9 \pm 1.5$  GPa with the pore size increase [Fig. 8(b)]. It coarsely obeys a linear decay with the pore size increase. The effect of the porosity on the mechanical properties of the Ti foams is shown in Figure 8(c and d). The plateau stress decreased from  $94.2 \pm 5.9$  to  $28.8 \pm 3.3$  MPa, and the Young's modulus decreased from  $36.1 \pm 3.5$  to  $6.2 \pm 1.8$  GPa with porosity increase. It generally obeys the rule of exponential decline with the porosity increase.

The plateau stress and Young's modulus coarsely obey linear declines with the pore size increase and exponential decline with the porosity increase. Liu<sup>[33]</sup> found that the plateau stress of the porous hydroxylapatite ceramics decreases linearly with increasing macropore size for a given total porosity. In this study, we found the plateau stress and Young's modulus coarsely obey linear declines

with the pore size increase [Fig. 8(a and b)]. Rice RW<sup>[34]</sup> has proposed a function on the relationship of porosity with strength of porous solids,

$$\sigma = \sigma_0 \exp(-cp) \quad (3)$$

where  $\sigma_0$  is zero-porosity strength,  $\sigma$  the strength at pore volume fraction  $p$ , and the constant  $c$  is related directly to the pore characteristics such as pore shape and size. In this study, we used the same Ti powder and NaCl spacer material; therefore,  $\sigma_0$  and  $c$  can be considered as constant. According to the above function, the strength ( $\sigma$ ) should decrease exponentially as the pore volume fraction ( $p$ ) increases. Our results in Figure 8(c and d) are well in accordance with the above function.

It is reported that powder sintered pure Ti foams with porosity of 55–75% showed plateau stress and Young's modulus are in the range of 10–35 MPa and 3–6.4 GPa.<sup>[35]</sup> Plateau stresses of 30–65 MPa and Young's modulus of 1.2–2.8 GPa were reported for commercial Ti foams

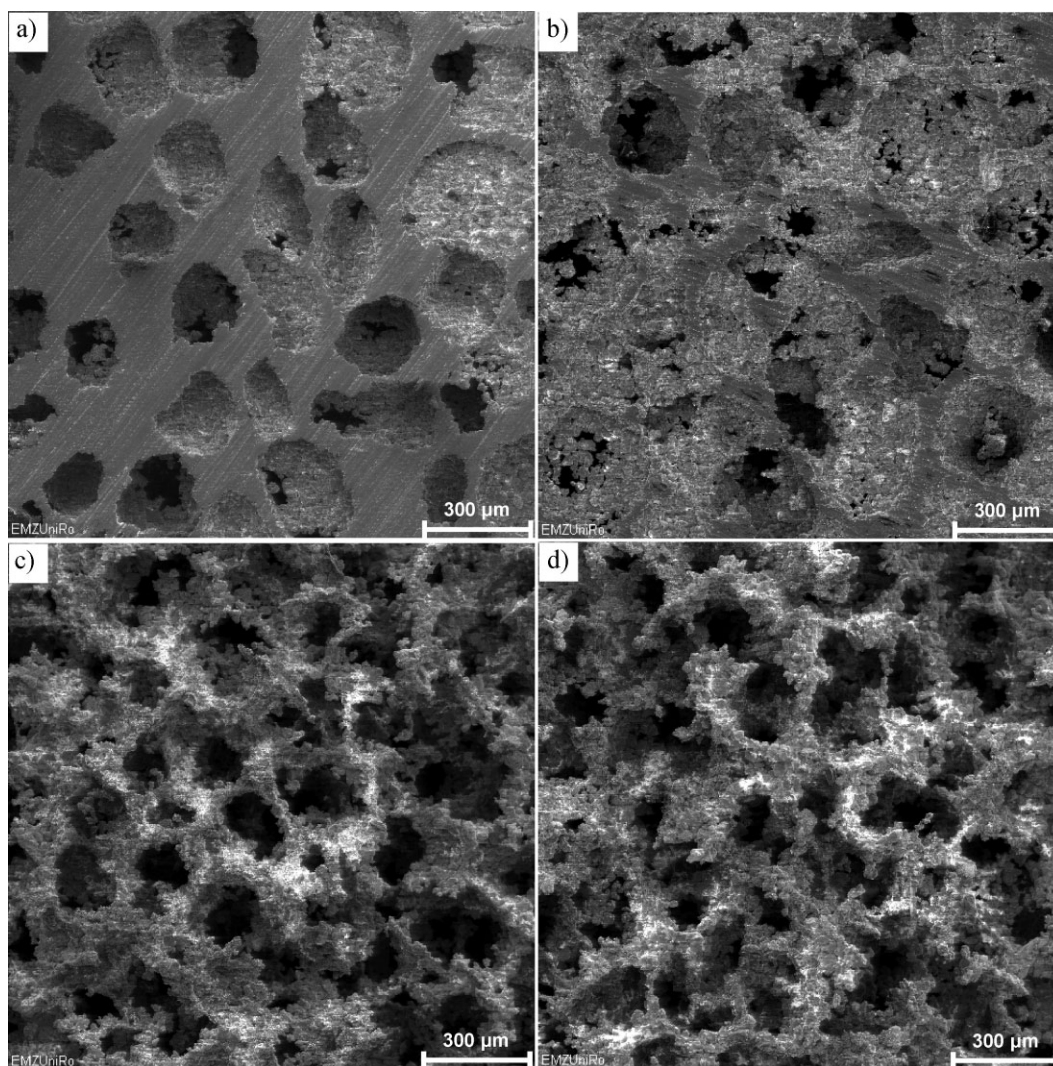


Fig. 6. SEM micrographs of the Ti foam surfaces with the same pore size of 250  $\mu\text{m}$  but different porosities of 30% (a), 45% (b), 55% (c), and 70% (d).

with 70–80% porosity produced by a solid sacrificial template.<sup>[36]</sup> Ti foams prepared by slip casting of particle stabilized emulsions showed yielding strengths of  $141 \pm 5.7$  and  $121 \pm 5.4$  MPa for samples with a porosity of 56.1 and 65.2%.<sup>[37]</sup> In this study, the 250  $\mu\text{m}$  pore sized Ti foams with 55% porosity shows plateau stress of  $45.1 \pm 3.0$  MPa and Young's modulus of  $13.46 \pm 1.4$  GPa. The same pore sized Ti foams with 70% porosity exhibit plateau strength of  $28.8 \pm 3.3$  MPa and Young's modulus of  $6.15 \pm 1.5$  GPa. The results are comparable to the reported values of the samples that prepared by powder sintered and solid sacrificial template foams, but lower than those of the slip casting of particle stabilized emulsions. The Ti powders used in this study are coarse particles in the range of 10–30  $\mu\text{m}$ . The sintering activity and density could be enhanced by ball milling of the raw Ti powders. It is believed that pure Ti foams with higher mechanical properties can be prepared by using the ball milling, SPS, and NaCl dissolution methods. Additionally, the phase

structure in these Ti foams is the low temperature  $\alpha$ -Ti phase but not the high temperature  $\beta$ -Ti phase because of the lower SPS temperature of 700  $^{\circ}\text{C}$ . The  $\beta$ -Ti phase has a cubic body centered crystalline structure, while the  $\alpha$ -Ti phase has a hexagonal crystalline structure which provides  $\beta$ -alloys with an improved notched fatigue resistance and a superior resistance to wear and abrasion.<sup>[38]</sup> The doping of  $\beta$  phase stabilized elements in Ti, for example Fe, V, Ta, Nb, Mn, Mo, Ni, Cr, Cu, etc. could decrease the phase transformation temperature from  $\alpha$  to  $\beta$  phase to below 700  $^{\circ}\text{C}$ .<sup>[39]</sup> It can be predicted that  $\beta$ -Ti alloy foams with much higher mechanical properties could be produced by using the SPS and NaCl dissolution methods.

Implants sometimes were used to substitute bone defects in tumor or spine surgery. Porous Ti foam with its osteoconductive properties is an ideal alternative bone graft. The porous structure with pore sizes of 200–500  $\mu\text{m}$  of the Ti foams may be able to permit bone cell penetration and tissue integration. The plateau stress of the human vertebral bone

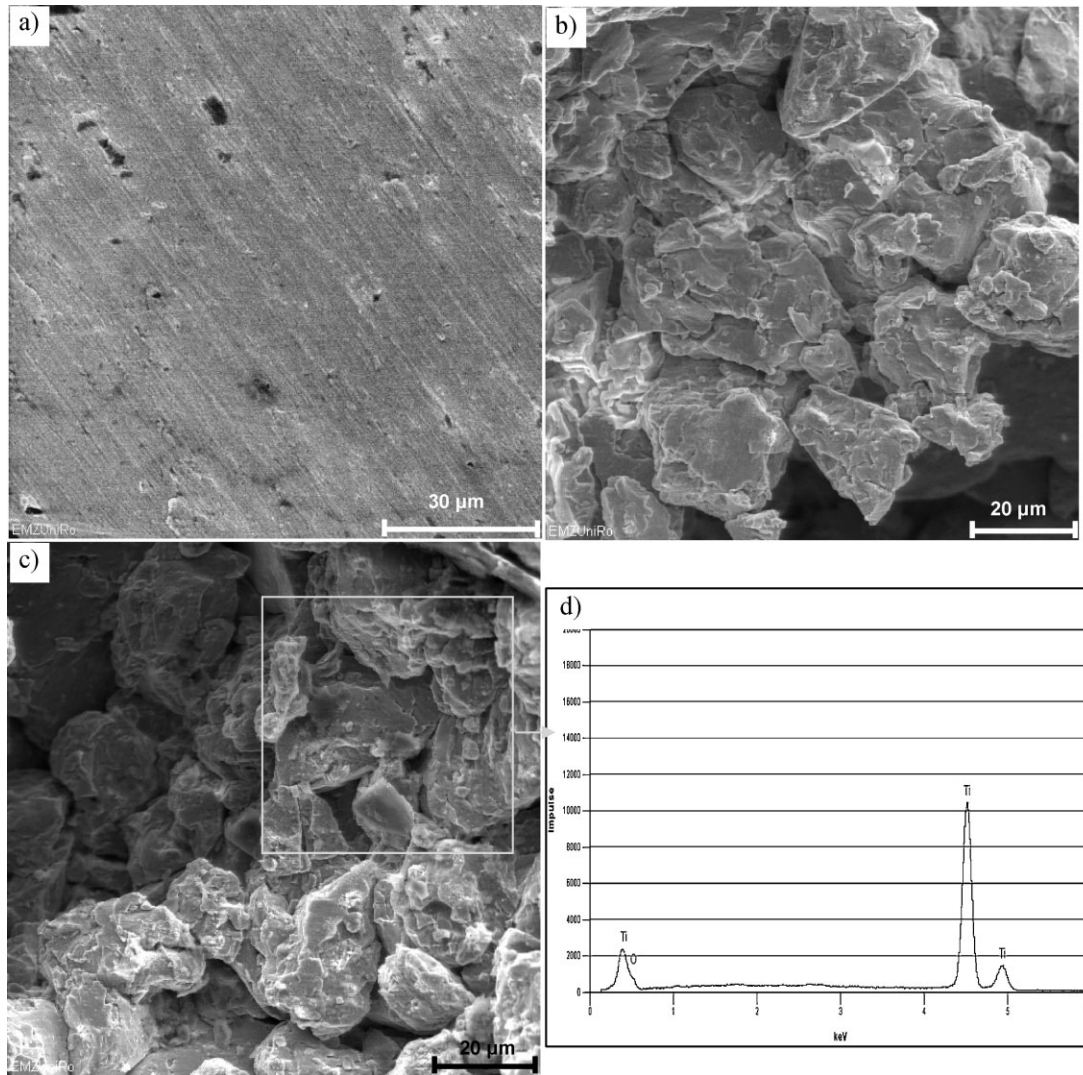


Fig. 7. SEM micrographs of the microstructure of the polished cross-section (a), pore edge (b), and pore wall (c) of the Ti foams, and EDX analysis on the pore matrix (d).

(load-bearing site) ranges from 24 to 43 MPa, and femoral cancellous bone (load-bearing site) is in the range of 48–80 MPa.<sup>[40]</sup> The average Young's modulus of compact bone of human ranges 7–30 GPa.<sup>[40]</sup> The plateau stress of the presented Ti foams in the range of 27.2–94.2 MPa is comparable to that of the cancellous bone which is enough for biomedical applications. For biomedical applications, the main problem of Ti and Ti alloys in clinical view is their high Young's modulus. Stress shielding is known to lead to bone resumption and eventual loosening of the implant.<sup>[41]</sup> The dense Ti generally showed much higher Young's modulus (70–120 GPa) than that of human bone. Thus, the porous structures were incorporated in the Ti and Ti alloys. In this study, the porous Ti foams show lower Young's modulus values (6.2–36.1 GPa) than that of dense ones which are comparable to those of natural compact bone (7–30 GPa). The macroporous Ti foams with plateau stress 27.2–94.2 MPa and Young's modulus 6.2–36.1 GPa have a potential to be used as bone implants. The low Young's modulus of Ti foams is

desirable to reduce the amount of stress shielding of the bone into which the foam is implanted. Combing the good biocompatibility of the pure Ti and the high interconnected porous structure, the Ti foams achieved by the SPS and NaCl dissolution methods with mechanical properties comparable to those of human bone makes these materials to be ideal bone implant foams.

In summary, macroporous pure Ti foams with porosities of 30–70% and pore sizes of 125–800 μm were prepared by using SPS and NaCl dissolution methods for bone implant applications. The Ti foams prepared by SPS at 700 °C for 8 min under 50 MPa showed pure α-Ti phase structure. The Ti foams consist of interconnected macropores with square cross sections. The plateau stress and Young's modulus agree with the Gibson–Ashby models, and coarsely obey linear declines with the pore size increase and exponential decays with the increase of porosity. The Ti foams processed by SPS and NaCl dissolution methods showed mechanical properties within those of human bone range.

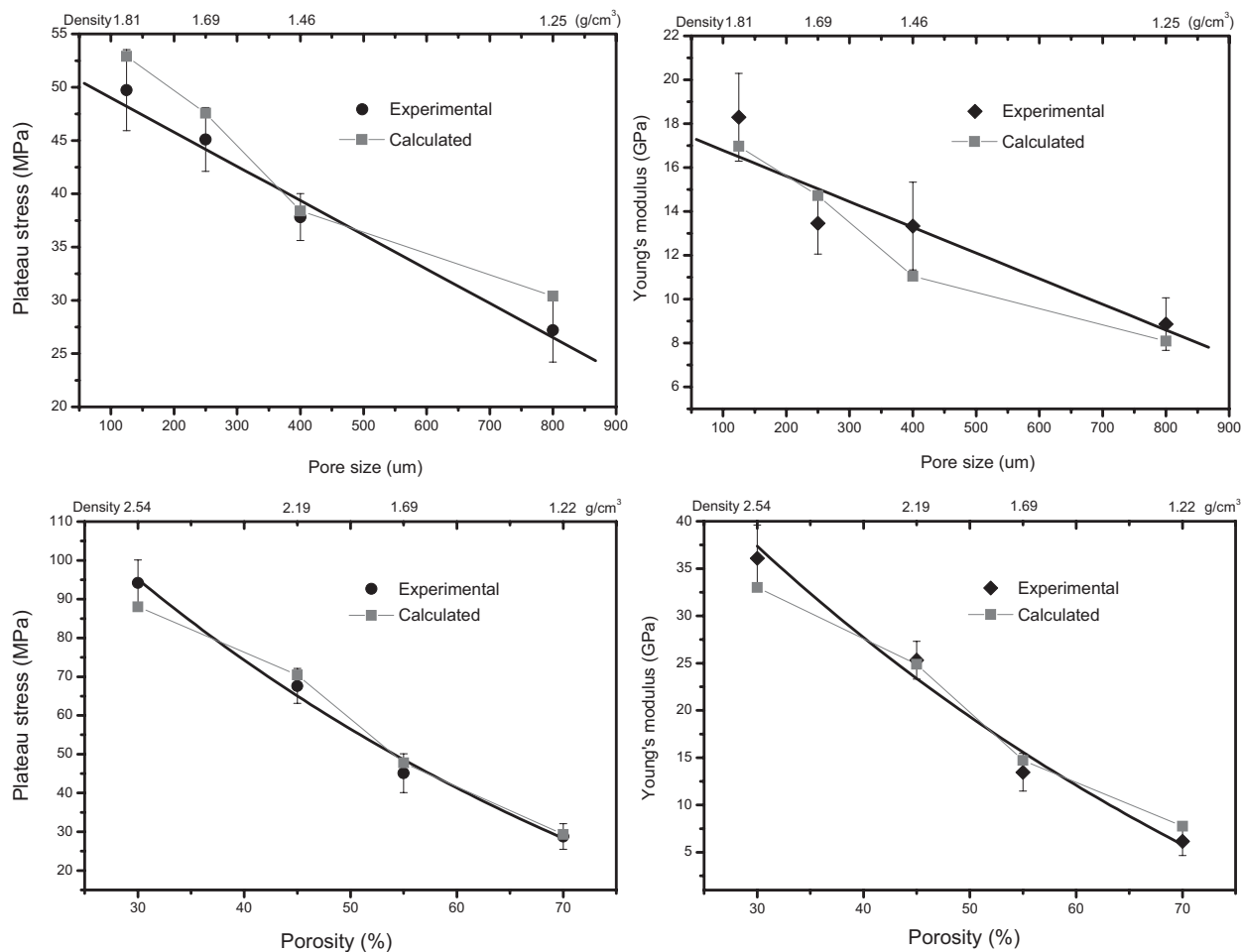


Fig. 8. The effects of pore sizes (a, b) and porosities (c, d) on the plateau stress and Young's modulus of the Ti foams.

Received: March 4, 2010  
Final Version: May 19, 2010

[1] A. G. Evans, J. W. Hutchinson, M. F. Ashby, *Prog. Mater. Sci.* **1999**, 3, 171.  
 [2] E. Solórzano, M. A. Rodriguez-Perez, J. A. de Saja, *Adv. Eng. Mater.* **2008**, 6, 596.  
 [3] J. Banhart, *Prog. Mater. Sci.* **2001**, 46, 559.  
 [4] J. P. Li, S. H. Li, C. A. Van Blitterswijk, K. de Groot, *J. Biomed. Mater. Res. A* **2005**, 73, 223.  
 [5] D. C. Dunand, *Adv. Eng. Mater.* **2004**, 6, 369.  
 [6] E. R. Garrett, S. P. Abhay, P. A. Dimitrios, *Biomaterials* **2008**, 27, 3625.  
 [7] Y. Chino, D. C. Dunand, *Acta Mater.* **2008**, 1, 105.  
 [8] Y. He, Y. Jiang, N. Xu, J. Zou, B. Huang, C. T. Liu, P. K. Liaw, *Adv. Mater.* **2007**, 19, 2102.  
 [9] B. Neirinck, T. Mattheys, A. Braern, J. Fransae, O. V. der Biest, J. Vleugels, *Adv. Eng. Mater.* **2009**, 8, 633.  
 [10] Y. B. An, N. H. Oh, Y. W. Chun, Y. H. Kim, J. S. Park, K. O. Choi, T. G. Eom, *Scr. Mater.* **2005**, 53, 905.

[11] R. Brindle, J. Eisenhauer, J. Rash, *PM<sup>2</sup> Industry vision and Technology Roadmap*. U.S. Department of Energy, Office of Industrial Technologies. **2001**, 9, 29.  
 [12] Z. A. Munir, U. Anselmi-Tamburini, *J. Mater. Sci.* **2006**, 41, 763.  
 [13] S. Grasso, Y. Sakka, G. Maizza, *Sci. Technol. Adv. Mater.* **2009**, 10, 053001.  
 [14] M. Kon, L. M. Hirakata, K. Asaoka, *J. Biomed. Mater. Res. B* **2004**, 68, 88.  
 [15] Y. Sakamoto, K. Asaoka, M. Kon, T. Matsubara, K. Yoshida, *Bio-Med. Mater. Eng.* **2006**, 2, 83.  
 [16] R. Nicula, R. Lüthen, M. Stir, B. Nebe, E. Burkel, *Biomolec. Eng.* **2007**, 24, 564.  
 [17] I. H. Oh, H. T. Son, C. S. Kang, J. S. Lee, J. I. Cho, J. C. Bae, B. T. Lee, H. Y. Song, *Mater. Forum* **2007**, 539–543, 635.  
 [18] T. Chandra, J. M. Torralba, T. Sakai, *Mater. Forum* **2003**, 426–424, 3079.  
 [19] M. Zadra, F. Casari, L. Girardini, A. Molinari, *Powder Metall.* **2008**, 51, 59.  
 [20] F. Zhang, J. Chang, K. Lin, J. Lu, *J. Mater. Sci. : Mater. Med.* **2008**, 19, 167.  
 [21] F. Zhang, K. Lin, J. Chang, J. Lu, C. Ning, *J. Euro. Ceram. Soc.* **2008**, 3, 539.

- [22] C. E. Wen, Y. Yamada, K. Shimojima, Y. Chino, H. Hosokawa, M. Mabuchi, *J. Mater. Res.* **2002**, *17*, 2633.
- [23] Y. Conde, J. F. Despois, R. Goodall, A. Marmottant, L. Salvo, C. S. Marchi, A. Mortensen, *Adv. Eng. Mater.* **2006**, *9*, 795.
- [24] A. Bansiddhi, D. C. Dunand, *Acta Biomater.* **2008**, *4*, 1996.
- [25] X. Zhao, H. Sun, L. Lan, J. Huang, H. Zhang, Y. Wang, *Mater. Lett.* **2009**, *28*, 2402.
- [26] C. E. Wen, M. Mabuchi, Y. Yamada, K. Shimojima, Y. Chino, H. Hosokawa, T. Asahina, *J. Mater. Sci. Lett.* **2003**, *20*, 1407.
- [27] M. Hakamada, Y. Yamada, T. Nomura, Y. Chen, H. Kusuda, M. Mabuchi, *Mater. Trans.* **2005**, *12*, 2624.
- [28] M. Hakamada, Y. Yamada, T. Nomura, Y. Chen, H. Kusuda, M. Mabuchi, *Appl. Phys. Lett.* **2006**, *88*, 254106.
- [29] K. Vanmeensel, A. Laptev, O. Van der Biest, J. Vleugels, *J. Euro. Ceram. Soc.* **2007**, *55*, 979.
- [30] K. Vanmeensel, A. Laptev, J. Hennicke, J. Vleugels, O. Van der Biest, *Acta Mater.* **2005**, *53*, 4379.
- [31] C. E. Wen, Y. Yamada, K. Shimojima, Y. Chino, T. Asahina, M. Mabuchi, *J. Mater. Sci.: Mater. Med.* **2002**, *13*, 397.
- [32] M. Long, H. J. Rack, *Biomaterials* **1998**, *19*, 1621.
- [33] D. M. Liu, *Ceram. Inter.* **1997**, *23*, 135.
- [34] R. W. Rice, *J. Mater. Sci.* **1993**, *8*, 2187.
- [35] W. Niu, C. Bai, G. Qiu, Q. Wang, *Mater. Sci. Eng. A* **2009**, *506*, 148.
- [36] A. Schuh, J. L. R. Vidael, W. Hoenle, T. Schmichal, *Materialwiss. Werkst.* **2007**, *12*, 1015.
- [37] B. Neirinck, T. Mattheys, A. Braem, J. Fransaer, O. Van der Biest, J. Vleugels, *Adv. Eng. Mater.* **2009**, *11*, 63.
- [38] E. Eisenbarth, D. Velten, M. Mueller, R. Thull, J. Breme, *Biomaterials* **2004**, *25*, 5705.
- [39] F. Zhang, A. Weidmann, J. B. Nebe, U. Beck, E. Burkel, *J. Biomed. Mater. Res.* **2010**, *94B*, 406.
- [40] F. Zhang, J. Chang, J. Lu, K. Lin, C. Ning, *Acta Biomaterialia* **2007**, *6*, 896.
- [41] M. Geetha, A. K. Singh, R. Asokamani, A. K. Gogia, *Prog. Mater. Sci.* **2009**, *3*, 397.